



UNIVERSITY OF LEEDS

This is a repository copy of *Experimental study of jet impingement heat transfer on a variable-curvature concave surface in a wing leading edge*.

White Rose Research Online URL for this paper:  
<http://eprints.whiterose.ac.uk/95740/>

Version: Accepted Version

---

**Article:**

Bu, X, Peng, L, Lin, G et al. (2 more authors) (2015) Experimental study of jet impingement heat transfer on a variable-curvature concave surface in a wing leading edge. *International Journal of Heat and Mass Transfer*, 90. pp. 92-101. ISSN 0017-9310

<https://doi.org/10.1016/j.ijheatmasstransfer.2015.06.028>

---

© 2015. This manuscript version is made available under the CC-BY-NC-ND 4.0 license  
<http://creativecommons.org/licenses/by-nc-nd/4.0/>

**Reuse**

Unless indicated otherwise, fulltext items are protected by copyright with all rights reserved. The copyright exception in section 29 of the Copyright, Designs and Patents Act 1988 allows the making of a single copy solely for the purpose of non-commercial research or private study within the limits of fair dealing. The publisher or other rights-holder may allow further reproduction and re-use of this version - refer to the White Rose Research Online record for this item. Where records identify the publisher as the copyright holder, users can verify any specific terms of use on the publisher's website.

**Takedown**

If you consider content in White Rose Research Online to be in breach of UK law, please notify us by emailing [eprints@whiterose.ac.uk](mailto:eprints@whiterose.ac.uk) including the URL of the record and the reason for the withdrawal request.



[eprints@whiterose.ac.uk](mailto:eprints@whiterose.ac.uk)  
<https://eprints.whiterose.ac.uk/>

# Experimental study of jet impingement heat transfer on a variable-curvature concave surface in a wing leading edge

Xueqin Bu<sup>1</sup> Long Peng<sup>2</sup> Guiping Lin<sup>1</sup> Lizhan Bai<sup>1,3,\*</sup> Dongsheng Wen<sup>3</sup>

<sup>1</sup> Laboratory of Fundamental Science on Ergonomics and Environmental Control, School of Aeronautic Science and Engineering, Beihang University, Beijing 100191, PR China

<sup>2</sup> Institute of Engineering Thermophysics, Chinese Academy of Sciences, Beijing 100190, PR China

<sup>3</sup> School of Chemical and Process Engineering, University of Leeds, Leeds, LS2 9JT, UK

**Abstract:** In this paper, extensive experimental investigation of the heat transfer characteristics of jet impingement on a variable-curvature concave surface in a wing leading edge was conducted for aircraft anti-icing applications. The experiments were carried out over a wide range of parameters: the jet Reynolds number,  $Re_j$ , from 51021 to 85340, the relative tube-to-surface distance,  $H/d$ , from 1.736 to 19.76, and the circumferential angle of jet holes on the piccolo tube,  $\theta$ , from  $-60^\circ$  to  $60^\circ$ . In addition, jet impingements with single one, two and three rows of aligned jet holes were all investigated. Experimental results revealed the effects of various parameters on the performance and characteristics of jet impingement heat transfer in the specific structure adopted here, and our insufficient understanding on the corresponding physical mechanism was presented. It was found that the jet impingement heat transfer performance was enhanced with the increase of jet Reynolds number. For single one row of jet holes, an optimal  $H/d$  of 4.5 was determined under  $Re_j = 51021$  and  $d = 2\text{mm}$ , for which the jet impingement achieved the best heat transfer performance. For two and three rows of aligned jet holes, the  $Nu_x$  curves in the chordwise direction exhibited much different shapes due to different intensity of the interference between adjacent air jets. This work contributes to a better understanding of the jet impingement heat transfer on a concave surface in a wing leading edge, which can lead to optimal design of the aircraft anti-icing system.

**Keywords:** jet impingement; concave surface; convective heat transfer; wing anti-icing

---

\* Corresponding author. Tel.: +86 10 8233 8600; Fax: +86 10 8233 8600

E-mail address: bailizhan@buaa.edu.cn (L. Bai)

## 1 Introduction

Jet impingement refers to a fluid stream issuing from a nozzle or slot and impinging on a flat or curved surface at a high velocity. As an effective method to enhance local heat transfer performance, jet impingement is adopted in a wide variety of fields, such as in the glass tempering, metal annealing, food and paper drying, gas turbine blade and electronics cooling. Jet impingement is a very complex heat and mass transfer phenomenon, which is influenced by many parameters including the shape and diameter of the nozzle, the nozzle layout, the nozzle to target surface distance, the jet Reynolds number, the impinging angle, the curvature of impinging surface, etc.

As jet impingement promises better heat transfer performance, it has attracted worldwide interest for decades. Both numerical simulation and experimental studies have been conducted to investigate the inherent physical mechanism, which is briefly reviewed below. At early stage, most of the studies focused on jet impingement on a flat surface. Early researchers such as Gardon [1], Hrycak [2] and Goldstein [3] concentrated on the influence of the nozzle-to-surface distance and jet Reynolds number on the heat transfer performance. The existence of an optimal nozzle-to-surface distance was found to reach the best heat transfer performance at the stagnation point. Gardon et al.[1] proposed that this optimal distance was equal to the length of the jet potential core, which was experimentally measured by Hrycak et al.[2]. Meanwhile, Hrycak pointed out that the length of the potential core and the Reynolds number were largely independent in the turbulent flow region.

Goldstein et al.[3] investigated the variation of Nusselt number at the stagnation point ( $Nu_{stag}$ ) at different  $H/d$  values, i.e. the ratio of the nozzle-to-surface distance to the jet hole diameter, and showed that: 1) At small  $H/d$  values, there existed secondary maxima for the local Nusselt number, which might be higher than that at the stagnation point,  $Nu_{stag}$ , due to the entrainment caused by the vortex rings in the shear layer; 2) The  $Nu_{stag}$  increased with the increase of  $H/d$ , and reached the maximum at  $H/d = 8$  because of the penetration of turbulence-induced mixing from the shear layer; 3) Once  $H/d$  was larger than 8, the  $Nu_{stag}$  decreased with further

increase of  $H/d$  due to a lower impinging velocity of the jet. The jet impingement with much smaller nozzle-to-surface distances ( $H/d \leq 0.25$ ) was studied by Lytle and Webb [4]. The local maximum of Nusselt number was also observed near the stagnation point, which increased remarkably with the decrease of the nozzle-to-surface distance and the increase of the jet Reynolds number. O'Donovan and Murray [5] obtained similar results through experimental research of jet impingement on a flat plate ( $0.5 \leq H/d \leq 8$  and  $10000 < Re < 30000$ ), and ascribed those secondary peaks in the radial distribution to an abrupt increase in the turbulence in the wall jet.

Wall pressure and wall shear stress of oblique jet impingement on a flat plate were studied both experimentally and analytically by Beltaos [6] in the jet impinging region and the wall jet region, which indicated that the flow was quasi-axisymmetric and the stagnation point removed from the jet center corresponded to the distribution of wall pressure. Sparrow and Lovell [7] investigated the influence of oblique angle ( $\alpha$ ) ranging from  $90^\circ$  (normal impingement) to  $30^\circ$ , by using the naphthalene sublimation technique. The results showed that the local heat transfer coefficient reached the maximum at  $\alpha = 90^\circ$ . While when  $\alpha$  was dropped to  $30^\circ$ , the local heat transfer coefficient decreased by 15 to 20 percent. The decrease of local heat transfer coefficient on the uphill side was faster than that on the downhill side, creating an imbalance of heat transfer that was more pronounced at smaller incident angles. Goldstein et al. [8] and Yan et al. [9] obtained visual results of the oblique jet impingement on a flat plate by using the temperature-sensitive liquid crystal technique. Yan et al. [9] compared the local Nusselt number distribution with different nozzle-to-surface distances. As the distance became smaller, the asymmetry of heat transfer distribution became more pronounced. Recently, O'Donovan and Murray [10] reported that both the stagnation point location and the location of the peak heat transfer coefficient were mainly dependent on the impingement angle instead of the nozzle-to-surface distance ( $30^\circ \leq \alpha \leq 90^\circ$  and  $2 \leq H/d \leq 8$ ), which was consistent with the results from Attalla and Salem[11].

All of these researches mentioned above provided valuable information about the heat transfer performance and characteristics of jet impingement on a flat plate. However, in some special applications, jet impingement heat transfer on a concave surface is necessary, and a typical example is for the gas turbine blade cooling. Metzger et al. [12] firstly performed an experimental study on a single row of circular jets impinging on a concave cylindrical surface. The results indicated that the optimal  $H/d$  value was 3~5 when  $Re$  ranged from 1150 to 5500. The optimal  $H/d$  value decreased with increasing Reynolds number. Yang et al. [13] investigated the slot jet impingement on a semi-circular concave surface, and three nozzle shapes including round, rectangular and 2-D contoured nozzles were considered. The secondary peak for heat transfer coefficient was also observed at small  $H/d$  values. The average heat transfer rates for impingement on the concave surface were found to be much higher than that on the flat plate, which was attributed to the effect of curvature. In the same year, the effect of concave surface curvature on round impinging jet was studied by Lee et al. [14], showing that Nusselt numbers at both the stagnation point and wall jet region increased with increasing surface curvature. The thinning of the boundary layer and the generation of Taylor-Görtler vortices might be the reasons responsible for such an enhancement. Gau et al. [15] and Cornaro et al. [16] presented the flow visualization of jets impinging on both convex and concave surfaces. Gau et al. [15] believed that the Taylor-Görtler vortices enhanced the momentum and energy exchange and strengthened thermal performance of jet impingement on concave surfaces, thus resulting in the increase of Nusselt number. Cornaro et al. [16] observed that the flow along the concave surface was less stable, and the vortex structures became fewer as the relative curvature increased.

3-D temperature distribution of a concave semi-cylindrical surface was measured by Fenot [17] using the infrared thermography. An interesting view of the effects of curvature was presented: the concavity effect similar to the comprehensions of Lee et al. [14] and Gau and Chung [15] could enhance the heat transfer, resulting in an increased local Nusselt number near the stagnation point at higher curvatures, however, comparing with the flat

plate case, the confinement effect would reduce the heat transfer and result in a lower Nusselt number. Öztekin et al. investigated the hydrodynamics and heat transfer characteristics of slot jet impingement on a concave surface [18, 19]. Results indicated that in contrast to the situation for a flat plate, the mean heat transfer coefficient along the concave surface would be larger only in a certain curvature range ( $R/L \geq 0.725$ , where R was the radius of the concave surface and L was the chord length of the concave surface). Meanwhile, the optimal relative curvature was obtained at  $R/L = 1.3$ .

To guarantee the aviation flight safety, anti-icing or de-icing system is indispensable for both civil and military aircraft, and hot-air anti-icing system has been widely employed so far. Fig.1 shows the schematic of a typical wing hot-air anti-icing system [20]. When the aircraft is flying under the icing conditions, high temperature and high pressure air from the engine compressor is introduced into the wing anti-icing cavity through the holes on the piccolo tube. The air jet increases the target surface temperature to ensure that no icing occurs in the wing leading edge, and it vents from a slot to the ambient through the exhaust holes.

Fig.2 shows the schematic view of the array jet impingement on a concave surface in the wing hot-air anti-icing system. Comparing to the common array jet impingement on a flat plate, there are some notable differences, as summarized below: 1) the supplied air pressure in the wing hot air anti-icing system is much higher, and the air in the jet holes is in the choked state with the outlet velocity approaching the speed of sound; 2) the jet hole profile is very sharp, and the air at the outlet of the jet hole is still under expansion; 3) the piccolo tube employed usually has single one, two or three rows of jet holes, and the jet inclination circumferentially along the piccolo tube can significantly affect the fluid flow and heat transfer process on the target surface; 4) for piccolo tube with two or three rows of jet holes, the interaction of jets from adjacent holes further increases the complexity of jet impingement heat transfer.

For the hot-air anti-icing system in a wing leading edge, the jet impingement process is much more complicated

than that of a concave cylindrical surface because the curvature of the inner surface of anti-icing cavity along the chordwise direction changes continuously caused by the airfoil geometry. Only a very limited work has been reported to date. Fregeau and Saeed [21-23] simulated the thermal performance of 3-D hot-air array jets impinging on a normal semicircular concave surface instead of the real inner surface of an anti-icing cavity. Results showed that the spacing between the two adjacent jet holes, the distance between the piccolo tube and the target surface, the array form of jet holes and jet mach number were the main parameters affecting the thermal performance. Meanwhile, the results indicated that the single array jets and the array jets with a 20 degree stagger yielded better heat transfer performance than that of the 10 degree stagger [22]. The thermal performance was enhanced with a larger jet hole pitch, a smaller distance between the piccolo tube and the target surface and a larger mach number. Among those, the distance between the piccolo tube and the target surface was the main influencing factor, but the optimized value was not reported [23].

Planquart et al. [24] obtained the heat transfer coefficient distribution on the inner surface of the anti-icing cavity with crossing jet piccolo tube through IR thermometer and the reverse heat transfer method. The results showed that the thermal performance was related to the jet Reynolds number and the chordwise and spanwise distances of adjacent jet holes. In addition, a correlation for the mean heat transfer coefficient in the peak-to-peak area was proposed by considering the air supply, the chordwise and spanwise distances of adjacent jet holes and rows of arrayed jet holes. Papadakis and See-Ho [25-27] investigated experimentally the influence of piccolo tube design and layout, the diffuser shape, hot air mass flowrate and temperature on the system performance and efficiency. They pointed out that once the air supply through the jet holes was choked, air supply mass flux had less influence on the anti-icing surface temperature than that of air supply temperature. The effects of piccolo tube layout and circumferentially arrayed form of the jet holes were significant in controlling the anti-icing surface temperature, but the cavity shape had negligible effect.

Based on the experimental data, Brown et al. [28] developed a correlation for the mean convective heat transfer coefficient on the front surface of a hot-air anti-icing cavity, where the parameters of jet hole spacing and the jet Reynolds number were considered. In the experiments, the air flowing from the jet holes was always kept choked, and the relative piccolo tube-to-surface distance ( $H/d$ ) was fixed at 5. More recently, Imbriale et al. [29] studied jet impingement heat transfer on a wing leading edge using the infrared thermal imaging technique. The influences of jet angle, jet hole spacing and Reynolds number on jetting heat transfer impinging on a concave surface were analyzed. The presence of stream-wise vortices was observed, which was influenced by the surface curvature, jet hole spacing and jet angle, and modified heat transfer correlations over the impinging area was proposed .

As summarized above, jet impingement heat transfer in a real wing anti-icing system is a very complex physical process, which is still lack of sufficient experimental data especially on the effects of variable surface curvature and multiple rows of jet holes on the hot-air jet heat transfer characteristics. In order to obtain reliable design parameters for a piccolo tube anti-icing system with more than one row of jet holes for which the study is quite limited, extensive experimental investigation is indispensable, which forms the motivation of this work.

## **2 Experimental setup**

Fig. 3 shows the experimental setup used in this study. It consists of an air supply system, a test unit including an anti-icing cavity and piccolo tubes, a heating system and a data measurement and acquisition system. The air supply system is composed of the air compressor, dry filter, buffer tank, temperature control module and some connection pipes providing high pressure air with fixed temperature for the test section. The air mass flowrate, temperature and pressure were measured by a gas flow meter, type T thermocouples and pressure transmitters, respectively.

As shown in Fig.4, the anti-icing cavity is designed as a detachable assembly, so that it can be equipped with different piccolo tubes at different locations conveniently. Before the experiments, the anti-icing cavity was

assembled with two side panels, and four fastening rods were used to ensure air tightness, so that the air can only exit from the exhaust holes. Different piccolo tubes can be installed in the cavity via the through hole in the left side panel, and accurate positioning was achieved by the positioning pin in the piccolo tube and the positioning hole in the right side panel. Meanwhile, the desired tube-to-surface distance  $H$  can be adjusted by replacing the left side panel with different through hole locations.

The 2-D profile of the anti-icing cavity adopted in the experiments is shown in Fig.1. The material of the cavity was aluminum-magnesium alloy (5A06), the thickness of the aluminum casing was 3.0mm, and the spanwise length of the cavity was 500mm. The piccolo tube was made of stainless steel with wall thickness of 1.5mm. The jet holes in the piccolo tube are shown in Fig.5. The jet hole was normal to the tube surface with a sharp edge. Three array patterns of the jet holes in the piccolo tube were investigated, i.e. single one, two or three rows of aligned jet holes, as shown in Fig.6.

A thin film electrical heater made of constantan was attached closely to the outer surface of the leading edge of the anti-icing cavity to provide a uniform heat flux of about  $5600 \text{ W/m}^2$ , which was measured by a power meter. Rubber sponge insulation materials with the thickness of about 10 cm were employed to cover the thin film heater in order to minimize the heat loss to the ambient, and the heat loss was estimated to be within 2.40%, which can be safely neglected. The temperature distribution on the internal surface of the leading edge of the anti-icing cavity was measured by the calibrated type T thermocouples. The thermocouple junctions were placed in the blind holes with a depth of 2.5mm in the outer surface and fixed by adhesives with good heat conduction and electrical insulation. Because all the thermocouple wires were arranged outside the anti-icing cavity, the flow field in the cavity was not affected. As the thermocouple junctions were placed only 0.5mm from the inner surface of the leading edge, it can accurately represent the temperatures at the inner surface. Fig.7 shows the detailed thermocouple arrangement along the chordwise direction of the leading edge. As the heat transfer in the stagnation

region is more complex, much denser measurement points were arranged. All the temperature data were acquired by the Agilent 34970 module and stored in the computer. The parameter ranges in the experiments are listed in Table 1.

### 3 Data Processing

The inverse heat transfer method was adopted in the experiment, i.e. heat is transferred to the wing anti-icing cavity, just opposite to the actual situation where heat is transferred from the wing anti-icing cavity. In order to investigate the flow and heat transfer in the wing anti-icing cavity, the outer surface of the leading edge of the anti-icing cavity was heated with a constant heat flux, and high pressure air with a fixed temperature of 300K was introduced into the cavity as a cooling medium.

Based on the experimental principle in this paper, the local convective heat transfer coefficient can be represented as:

$$h_x = \frac{q}{T_{wx} - T_{in}} \quad (1)$$

where  $q$  is the heat flux at the outer surface of the leading edge;  $T_{wx}$  is the local temperature at the inner surface of the leading edge and  $T_{in}$  is the inlet temperature of the supplied air.

Note that, in the calculation of the local convective heat transfer coefficient, we did not take into account the tangential thermal conduction in the wall, so the results obtained here would deviate from the actual ones to some extent. However, as our anti-icing cavity model simulated the real one in practical application including both the structure and material, so we can adopt our experimental results to guide the anti-icing cavity design without considering the tangential thermal conduction effect of the wall, which will make the design process more convenient.

The local Nusselt Number can be expressed by equation (2):

$$\text{Nu}_x = \frac{h_x d}{\lambda} \quad (2)$$

where  $d$  is the diameter of the jet hole and  $\lambda$  is the thermal conductivity of air.

The jet Reynolds Number is defined by Equation (3):

$$\text{Re}_j = \frac{\frac{G_m}{N\rho\pi(d/2)^2} d}{\nu} = \frac{4G_m \times d}{\rho N \pi d^2 \left(\frac{\mu}{\rho}\right)} = \frac{4G_m}{N\pi d \mu} \quad (3)$$

where  $G_m$  is the mass flowrate of air,  $N$  is the number of jet holes,  $\rho$  is the density of air,  $\mu$  and  $\nu$  are the kinetic and dynamic viscosities, respectively.

Table 2 presents the measurement uncertainties of the directly measured parameters, such as the voltage, resistance, temperature and flow rate. Based on the data in Table 2, the uncertainties of both  $h$  and  $\text{Nu}$  were smaller than 5.0%.

#### 4 Comparison and validation of the experimental results

To validate the experimental results obtained in this work, it is necessary to make a comparison with other existing experimental data. Because the test model in this paper represents a real wing anti-icing system equipped on a regional jet, while most published experimental and numerical results were achieved for flat or cylindrical surface, it is difficult to find an appropriate example to compare with our results. The only possible example for comparison is found from the work by Brown et al [28], who experimentally investigated a full-scale, 2-D model of an aircraft nacelle anti-icing system. The profile of the impingement surface as well as the operating conditions from Ref. [28] is similar to those in this paper, and Fig.8 shows the comparison between our results and those from Brown et al. In the experiment from Brown et al.,  $d=1.5\text{mm}$ ,  $H/d=5$ , while in our experiment,  $d=2\text{mm}$ ,  $H/d=6.63$ . As shown in Fig.8, our experimental results for averaged Nusselt number exhibit similar trend with those from Brown et al., but are a little lower caused by a higher relative tube-to-surface distance in our experiment. This comparison validates the accuracy of the experimental results in this paper.

## 5. Experimental Results and Discussions

### 5.1 Influence of jet Reynolds number

Fig.9 (a) and (b) illustrate the influence of jet Reynolds number  $Re_j$  on the heat transfer distribution on the impinging surface in the chordwise direction with two and three rows of aligned jet holes, respectively. As shown in Fig.9,  $Re_j$  has significant impacts on the convective heat transfer performance on the whole impinging surface including both the jet impingement region and the wall jet region. For both jet hole layouts, the larger the jet Reynolds number, the higher the heat transfer performance. That is because a higher jet Reynolds number corresponds to a larger jet velocity, and the higher turbulence level inherited from the upstream of the nozzle exit or developed in the jet flow field by the shear-driven interaction with the ambient air contributes greatly to the heat transfer enhancement. This result is in agreement with those presented in other papers [29-30].

The comparison between Fig.9 (a) and Fig.9 (b) shows that the number of rows of aligned jet holes also has important effect on the heat transfer distribution in the chordwise direction of the impinging surface. The  $Nu_x$  curves for two rows of aligned jet holes have two peaks with a valley between them. However, for the case of three rows, only one peak appears in the middle of the  $Nu_x$  curves. It is believed that the relative jet interference is responsible for the result. For two rows of aligned jet holes, the chordwise distance between adjacent jets is relatively large, and the jet interference effect is small, which produces two independent peaks and one valley. However, for three rows of aligned jet holes, the reduced chordwise distance increases jet interference, resulting in the enhancement of the heat transfer around the centre of the two adjacent stagnation points. For the  $Nu_x$  curves with both two and three rows of aligned jet holes, the peak value increases with the increase of the jet Reynolds number, but the peak position remains unchanged.

### 5.2 Influence of relative tube-to-surface distance

Fig.10 shows the influence of  $H/d$  value, i.e. the ratio of the tube-to-surface distance to the jet hole diameter, on

the heat transfer distribution in the chordwise direction of the impinging surface, and Fig.10 (b) is the local enlargement of the stagnation region in Fig.10 (a). In the experiment, the jet hole diameter was kept as 2mm, the Reynolds number was 51021, the H/d value was varied from 2.5 to 9.88, and the piccolo tube had one row of aligned jet holes. For a fixed H/d value, the heat transfer performance peaked around the stagnation region and decreased rapidly as it is away from the stagnation point. The heat transfer performance on the impinging surface increased with increasing H/d values as  $H/d < 4.5$ , but decreased as  $H/d > 4.5$ . It indicates that there exists an optimal H/d value to realize the best heat transfer performance on the impinging surface, and for the specific structure adopted here, the optimal H/d value is found to be 4.5.

When the relative tube-to-surface distance H/d is smaller than 4.5, the jet arriving at the impinging surface is not fully developed, and a potential core region exists in front of the target surface. As H/d decreases, the travelling distance of the jet decreases accordingly, and the shear-driven interaction between the jet and the surrounding air becomes quite limited, resulting in the drop of the local  $Nu_x$  in the stagnation zone due to the decrease of the jet turbulence level. When the H/d is larger than 4.5, the jet is fully developed before impinging onto the target surface. Under this condition, the target surface is in the downstream zone of the potential core. As H/d increases, the distance between the jet holes and the impingement surface increases accordingly, and the momentum and velocity in the jet core zone drops gradually because of the shear-driven interaction between the jet and the surrounding air, resulting in the decrease of the heat transfer in the stagnation zone of the target surface.

As shown in Fig.10 (b), for  $H/d = 2.5$ , two weak peaks in the  $Nu_x$  curve are observed at location  $x/d = \pm 2$  corresponding to the upper and lower surface of the wing, with a valley centered at the stagnation point. According to Ref.[31], the peak located at radial distance of about  $2d$  from the jet axis, is not so readily explained and motivated a huge amount of both experimental and computational researches until the very recent days. A

reasonable explanation is from Meola et al. [32], who gave an experimental evidence to conclude that the vortex ring surrounding the jet was responsible for the Nusselt number peak located at radial distance of about  $2d$  from the jet axis. This phenomenon can be considered a result of flow reattachments after flow separation and not of a simple transition from laminar to turbulent flow.

Fig. 11 and Fig. 12 show the influence of  $H/d$  on  $Nu_x$  distribution in the chordwise direction for two and three rows of jet holes, respectively. As shown in Fig. 11 and Fig. 12, the relative tube-to-surface distance  $H/d$  has significant effect on the jet impingement heat transfer performance and characteristics. The heat transfer performance decreases with the increase of the relative tube-to-surface distance  $H/d$ , however, the shape of the  $Nu_x$  curve does not change with the variation of  $H/d$ . The corresponding physical mechanism is similar to that in Fig.10, which are not repeated here.

### 5.3 Influence of circumferential angle of jet holes on the piccolo tube

Fig.13 illustrates the definition of the circumferential angle of jet holes on the piccolo tube, and Fig.14 (a-c) shows the influence of jet impingement angle  $\theta$  on the heat transfer distribution in the chordwise direction of the impinging surface for single one, two and three rows of aligned jet holes, respectively. Clearly the jet impingement angle  $\theta$  significantly affects the local  $Nu_x$  distribution in the chordwise direction. Taking Fig.14 (a) as an example, when the circumferential angle of jet holes on the piccolo tube  $\theta = 0^\circ$ , the optimal thermal performance is observed at the stagnation point A, and the peak value of  $Nu_x$  reaches 23. When  $\theta = 30^\circ$ , the peak value of  $Nu_x$  at the stagnation point A1 reaches 20, which drops by 13.0% compared to that when  $\theta = 0^\circ$ . When  $\theta = -45^\circ$ , the peak value of  $Nu_x$  at the stagnation point A2 reaches 19.2, which drops by 16.5% compared to that when  $\theta = 0^\circ$ . This is because the change of the circumferential angle of jet holes on the piccolo tube  $\theta$  leads to the variations of the curvature radius at the impinging point, jet impingement angle and jet hole-to-surface distance. The jet hole-to-surface distances in the three conditions above are almost the same, but the curvature radius at the

impinging point and the impingement angle differ substantially. For the circumferential angle of jet holes  $\theta = 0^\circ$ , the curvature radius at the stagnation point is much smaller than the other two conditions, while the impingement angle is the largest one ( $\alpha = 90^\circ$ ), resulting in the highest Nusselt number at the stagnation point for  $\theta = 0^\circ$ . This result is consistent with the experiment conducted by Gau and Chung[15]. The Nusselt number increases with increasing surface curvature at the stagnation point. This phenomenon is due to the Taylor-Görtler vortices, which can significantly increase the momentum and energy exchange near the wall, and enhance the heat transfer for flow over a concave surface, as supported by Mayle et al. [33] and Thomann [34]. The jet surface curvature at the stagnation point with  $\theta = 30^\circ$  is a little lower than that with  $\theta = -45^\circ$ , but the jet impingement angle with  $\theta = 30^\circ$  is much larger, resulting in a larger Nusselt number at the stagnation point with  $\theta = 30^\circ$ .

Moreover, when the circumferential angle of jet holes on the piccolo tube is fixed at  $\theta = 0^\circ$ ,  $30^\circ$  and  $-45^\circ$ , the variation trends of the corresponding  $Nu_x$  curves along the chordwise direction are much different, as shown in Fig.14 (a). For all the three circumferential angles, the  $Nu_x$  curves exhibit asymmetrical trend due to different surface slopes between the upper and lower sides. Especially for  $\theta = 30^\circ$  or  $-45^\circ$ , the Nusselt number on the uphill side is much larger than that on the downhill side. That is because the oblique jet leads to a main flow toward the uphill side of the impinging surface, and the flow toward the downhill side will be confined.

The circumferential angle of jet holes on the piccolo tube also affects the  $Nu_x$  distribution on the impinging surface in the chordwise direction with multiple rows of aligned jet holes, and Fig.14 (b) and (c) present the results for two and three rows of aligned jet holes, respectively. For two rows of aligned jet holes in Fig.14 (b), the circumferential angle of jet holes affects the double peak distribution on the  $Nu_x$  curve. As the circumferential angle of jet holes on the piccolo tube changes from  $\pm 15^\circ$  to  $\pm 45^\circ$  and further to  $\pm 60^\circ$ , the distance between the two peaks increases gradually, however, the averaged  $Nu_x$  between the two peaks decreases, and the difference between the peak and valley  $Nu_x$  becomes larger. The reason can be explained as follows: with the circumferential

angle of the jet holes decreasing, the two stagnation points gets closer, and the strong interaction between the two wall jets produces a complex flow structure, which enhances the heat transfer between the two stagnation points and results in a relatively large valley  $Nu_x$ . The heat transfer performance for three rows of aligned jet holes as shown in Fig.14 (c) is generally similar to that of Fig.14 (b), with an exception that the valley  $Nu_x$  disappears due to the addition of a row of aligned jet holes at  $\theta = 0^\circ$ .

## 6 Conclusions

This paper presents extensive experimental study of the jet impingement heat transfer on a variable-curvature concave surface in a wing leading edge for aircraft wing anti-icing applications. The influence of a variety of parameters that include the jet Reynolds number ( $Re_j$ ), relative tube-to-surface distance ( $H/d$ ), jet impingement angle ( $\theta$ ) and the number of rows of aligned jet holes on the jet impingement heat transfer performance and characteristics were investigated, and some important conclusions can be summarized as follows:

- 1) The jet Reynolds number ( $Re_j$ ) has significant effect on the jet impingement heat transfer on the whole impinging surface including both the stagnation zone and the wall jet zone, and the larger the jet Reynolds number, the higher the heat transfer performance.
- 2) For two rows of aligned jet holes, two peaks exist in the  $Nu_x$  curve in the chordwise direction due to the weak interference between each other, and the peak position does not change with the variation of jet Reynolds number; while for three rows of aligned jet holes, only one peak exists in the  $Nu_x$  curve in the chordwise direction due to strong interference between adjacent air jets.
- 3) For single one row of jet holes, with the increase of the relative tube-to-surface distance, the jet impingement heat transfer performance firstly increases, then decreases, and there exists an optimal value to achieve the best jet impingement heat transfer performance. For the experimental conditions in this work, the optimal value of  $H/d$  was determined as 4.5 under  $Re_j = 51021$  and  $d = 2\text{mm}$ .

4) Decreasing curvature radius and increasing jet impingement angle can both enhance jet impingement heat transfer performance at the stagnation point. At the same time, for oblique jet, the jet impingement heat transfer performance on the uphill side of the impinging surface is much better than that on the downhill side due to the flow confinement effect.

#### **ACKNOWLEDGEMENT**

This work was supported by the National Natural Science Foundation of China (Grant No. 51206008) and the EU Marie Curie Actions-International Incoming Fellowships (FP7-PEOPLE-2013-IIF-626576).

## References

- [1] R. Gardon, J. Cobonpue, Heat transfer between a flat plate and jets of air impinging on it, International Heat Transfer Conference, Pt. 2 (1961) 454-460
- [2] P. Hrycak, S. Jachna, D. T. Lee, A study of characteristics of developing, incompressible, axisymmetric jets, Lett. Heat Mass Transfer 1 (1974) 63-71
- [3] R. J. Goldstein, A. I. Behbahani, K. Heppelmann, Streamwise distribution of the recovery factor and the local heat transfer coefficient to an impinging circular air jet, Int. J. Heat Mass Transfer 29 (1986) 1227-1235
- [4] D. Lytle, B. W. Webb, Air jet impingement heat transfer at low nozzle-plate spacings, Int. J. Heat Mass Transfer 37 (1994) 1687-1697
- [5] T. S. O'Donovan, D. B. Murray, Jet impingement heat transfer - Part I: Mean and root-mean-square heat transfer and velocity distributions, Int. J. Heat Mass Transfer 50 (2007) 3291-3301
- [6] S. Beltaos, Oblique impingement of circular turbulent jets, Journal of Hydraulic Research 14 (1976) 17-36
- [7] E. M. Sparrow, B. J. Lovell, Heat transfer characteristics of an obliquely impinging circular jet, J. Heat Transfer Trans. ASME 102(1980) 202-209
- [8] R. J. Goldstein, M. E. Franchett, Heat transfer from a flat surface to an oblique impinging jet, J. Heat Transf. Trans. ASME 110 (1988) 84-90
- [9] X. Yan, N. Saniei, Heat transfer from an obliquely impinging circular, air jet to a flat plate, Int. J. Heat Fluid Flow 18 (1997) 591-599
- [10] T. S. O'Donovan, D. B. Murray, Fluctuating fluid flow and heat transfer of an obliquely impinging air jet, Int. J. Heat Mass Transfer 51 (2008) 6169-6179
- [11] M. Attalla, M. Salem, Experimental investigation of heat transfer for a jet impinging obliquely on a flat surface, Exp. Heat Transfer 28 (2015) 378-391

- [12] D. E. Metzger, T. Yamashita, C. W. Jenkins, Impingement Cooling of Concave Surfaces with Lines of Circular Air Jets, *J. Eng. Gas Turbines Power* 91 (1969) 149-155
- [13] G. Yang, M. Choi, J. S. Lee, An experimental study of slot jet impingement cooling on concave surface: effects of nozzle configuration and curvature, *Int. J. Heat Mass Transfer* 42 (1999) 2199-2209
- [14] D.H. Lee, Y.S. Chung, S.Y. Won, The effect of concave surface curvature on heat transfer from a fully developed round impinging jet, *Int. J. Heat Mass Transfer* 42(1999) 2489-2497
- [15] C. Gau, C.M. Chung, Surface curvature effect on slot-air-jet impingement cooling flow and heat transfer process, *J. Heat Transf. Trans. ASME* 113 (1991) 858-864
- [16] C. Cornaro, A. S. Fleischer, R. J. Goldstein, Flow visualization of a round jet impinging on cylindrical surfaces, *Exp. Therm. Fluid Sci.* 20 (1999) 66-78
- [17] M. Fenot, E. Dorignac, J.-J. Vullierme, An experimental study on hot round jets impinging a concave surface, *Int. J. Heat Fluid Flow* 29 (2008) 945-956
- [18] E. Öztekin, O. Aydin, M. Avcı, Hydrodynamics of a turbulent slot jet flow impinging on a concave surface, *Int. Commun. Heat Mass Transfer* 39 (2012) 1631-1638
- [19] E. Öztekin, O. Aydin, M. Avcı, Heat transfer in a turbulent slot jet flow impinging on concave surfaces, *Int. Commun. Heat Mass Transfer* 44 (2013) 77-82
- [20] V.J. Jusionis, Heat transfer from impinging gas jets on an enclosed concave surface, *Journal of Aircraft*, 7(1) (1970) 87-88
- [21] M. Fregeau, F. Saeed, I. Paraschivoiu and F. Saud, Numerical heat transfer correlation for array of hot-air jets impinging on 3-dimensional concave surface, *J. Aircr.* 42(3) (2005) 665-670
- [22] F. Saeed, Numerical simulation of surface heat transfer from an array of hot-air jets, *J. Aircr.* 45(2) (2008) 700-714
- [23] M. Fregeau, M. Gabr, I. Paraschivoiu, et al., Simulation of heat transfer from hot-air jets impinging a three-dimensional concave surface, *J. Aircr.* 46(2) (2009) 721-725

- [24] P. Planquart, G.V. Borre, J.M. Buchlin, Experimental and numerical optimization of a wing leading edge hot air anti-icing system, AIAA paper 2005-1277, 2005
- [25] M. Papadakis, S.J. Wong, Parametric investigation of a bleed air ice protection system, AIAA paper 2006-1013, 2006
- [26] M. Papadakis, S.J. Wong, H.W. Yeong, et al., Icing tunnel experiments with a hot air anti-icing system, AIAA paper 2008-444, 2008
- [27] M. Papadakis, S.J. Wong, H.W. Yeong, et al., Icing tests of a wing model with a hot-air ice protection system, AIAA Paper 2010-7833, 2010
- [28] J. M. Brown, S. Raghunathan, J.K. Watterson, et al., Heat transfer correlation for anti-icing systems. *J. Aircr.* 39(1) (2002) 65-70
- [29] M. Imbriale, A. Ianiro, C. Meola, et al., Convective heat transfer by a row of jets impinging on a concave surface. *Int. J. Therm. Sci.* 75(2014) 153-163
- [30] C. Meola, A new correlation of Nusselt number for impinging jets, *Heat Transfer Eng.* 30(3) (2009) 221-228
- [31] G.M. Carlomagno, A. Ianiro, Thermo-fluid-dynamics of submerged jets impinging at short nozzle-to-plate distance: A review, *Experimental Thermal and Fluid Science* 58(2014) 15-35
- [32] C. Meola, L. de Luca, G.M. Carlomagno, Influence of shear layer dynamics on impingement heat transfer, *Exp. Therm. Fluid Sci.* 13 (1996) 29-37
- [33] R.E. Mayle, M.F. Blair, F.C. Kopper, Turbulent boundary layer heat transfer on curved surfaces, *J. Heat Transfer Trans. ASME* 101 (1979) 521-525
- [34] H. Thomann, Effect of streamwise wall curvature on heat transfer in a turbulent boundary layer, *Journal of Fluid Mechanics* 33 (1968) 283-292

## Nomenclature

$C_n$	spanwise distance between adjacent jet holes, mm
$d$	jet hole diameter, mm
$D$	piccolo tube diameter, mm
$G_m$	Mass flowrate, g/s
$h_x$	local convective heat transfer coefficient, $W/(m^2 \cdot K)$
$H$	piccolo tube-to-surface distance, m
$N$	number of jet holes
$Nu_x$	local Nusselt number
$q$	heat flux, $W/m^2$
$r$	arc length between jet stagnation points, mm
$Re_j$	jet Reynolds number
$T_{in}$	supplied air temperature, K
$T_{wx}$	local temperature on internal surface of the wall, K
$\alpha$	jet impingement angle ( $^\circ$ )
$\rho_c$	curvature radius, m
$\rho$	density, $kg/m^3$
$\theta$	circumferential angle of jet holes on the piccolo tube ( $^\circ$ )
$\lambda$	thermal conductivity, $W/(m \cdot K)$
$\nu$	kinetic viscosity, $m^2/s$

**Table captions**

Table 1 Parameter range in the experiments

Table 2 Uncertainties of measuring equipments

## Figure captions

Fig. 1 Schematic of typical wing hot-air anti-icing cavity

Fig. 2 Schematic of jet impingement on a concave surface from a piccolo tube

Fig. 3 Photo of the experimental system

Fig. 4 Disassembly sketch of hot-air anti-icing cavity

Fig. 5 Structure of jet holes in piccolo tube

Fig. 6 Jet hole layout in the piccolo tubes

Fig. 7 Distribution of temperature measurement points

Fig. 8 Comparison and validation of the experimental results

Fig. 9 Influence of  $Re_j$  on  $Nu_x$  distribution in the chordwise direction

Fig. 10 Influence of  $H/d$  on  $Nu_x$  distribution in the chordwise direction for single one row of jet holes

Fig. 11 Influence of  $H/d$  on  $Nu_x$  distribution in the chordwise direction for two rows of jet holes

Fig. 12 Influence of  $H/d$  on  $Nu_x$  distribution in the chordwise direction for three rows of jet holes

Fig. 13 Illustration of the circumferential angle of jet holes on the piccolo tube

Fig. 14 Influence of circumferential angle of jet holes on  $Nu_x$  distribution in the chordwise direction

Table 1 Parameter range in the experiments

Structure parameters	Range
d (mm)	2
$\theta_{-1}, \theta_0, \theta_1$	$\theta_{-1}:(-60^\circ \sim -15^\circ), \theta_0:(-10^\circ \sim 10^\circ), \theta_1:(15^\circ \sim 60^\circ)$
H/d	1.736~19.76
r/d	8.1~50.2
Cn (mm)	50
number of rows of aligned jet holes	Single one, two or three

Table 2 Uncertainties of measuring equipments

Equipment	Accuracy grade	Measuring errors
Type T thermocouple	I	$\pm 0.004 T $
PT100 thermal resistance	II	$\pm(0.30 \pm 0.005 T )$
Pressure transmitter	II	$\pm 0.2\% F.S$
Standard 24-volt outlet	II	0.2%
Air mass flow meter	II	$\pm 0.2\% F.S$

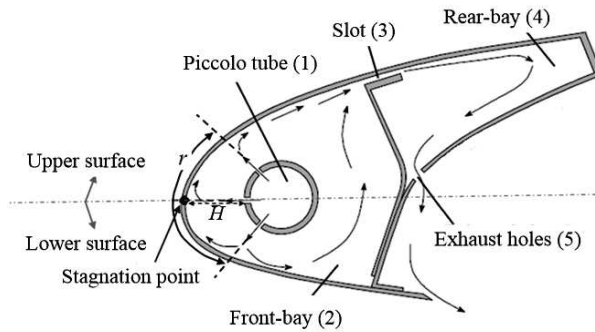


Fig. 1 Schematic of typical wing hot-air anti-icing cavity

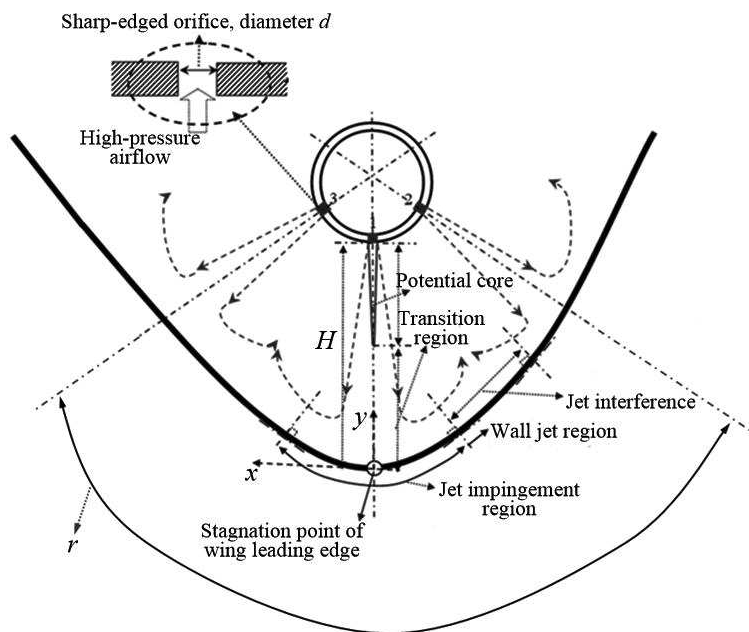


Fig. 2 Schematic of jet impingement on a concave surface from a piccolo tube

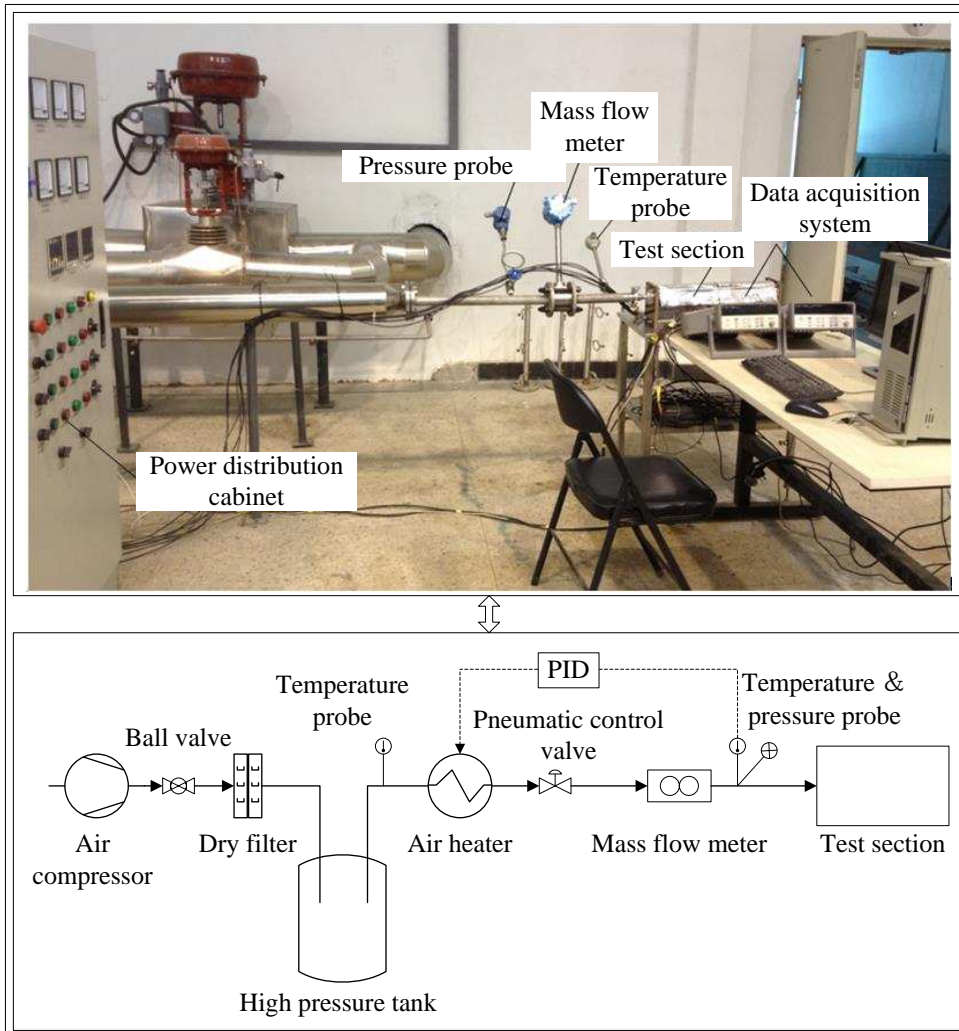


Fig. 3 Photo of the experimental system

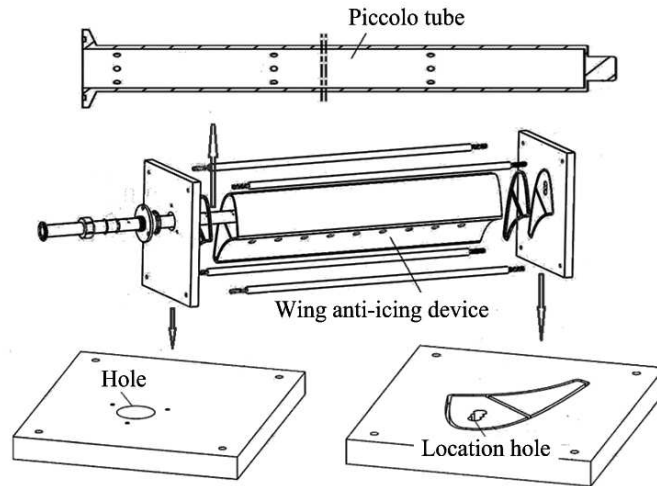


Fig. 4 Disassembly sketch of hot-air anti-icing cavity

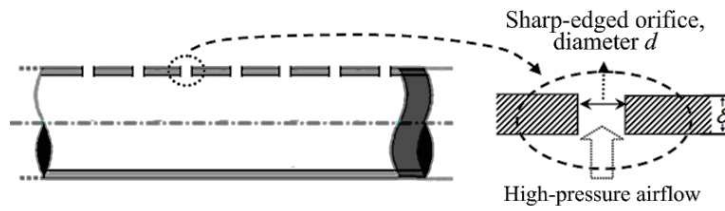


Fig. 5 Structure of jet holes in piccolo tube

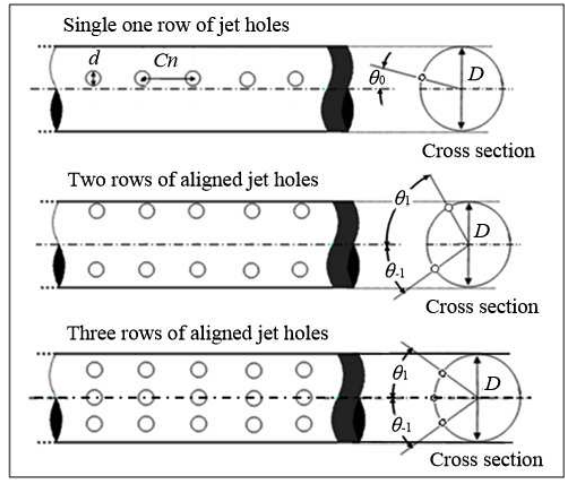


Fig. 6 Jet hole layout in the piccolo tubes

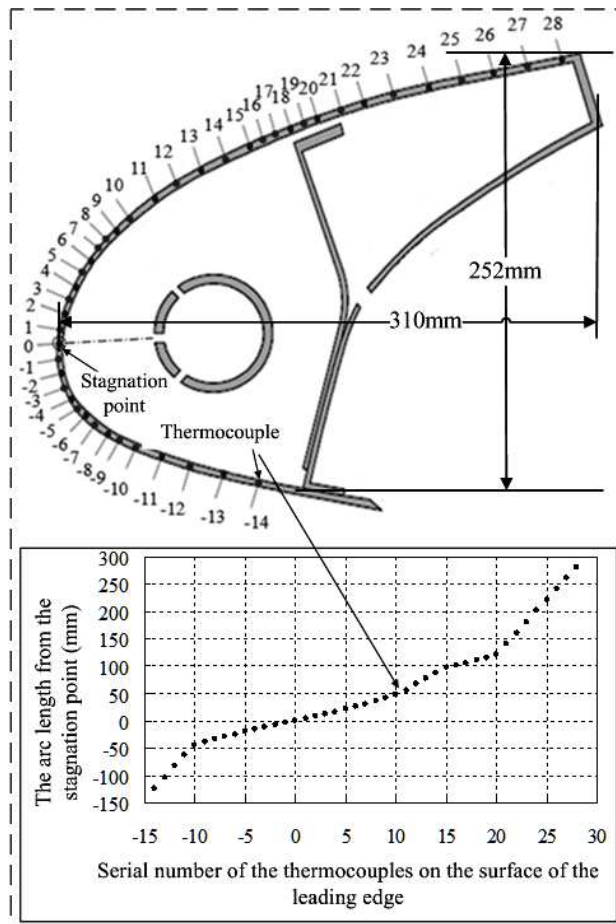


Fig. 7 Distribution of temperature measurement points

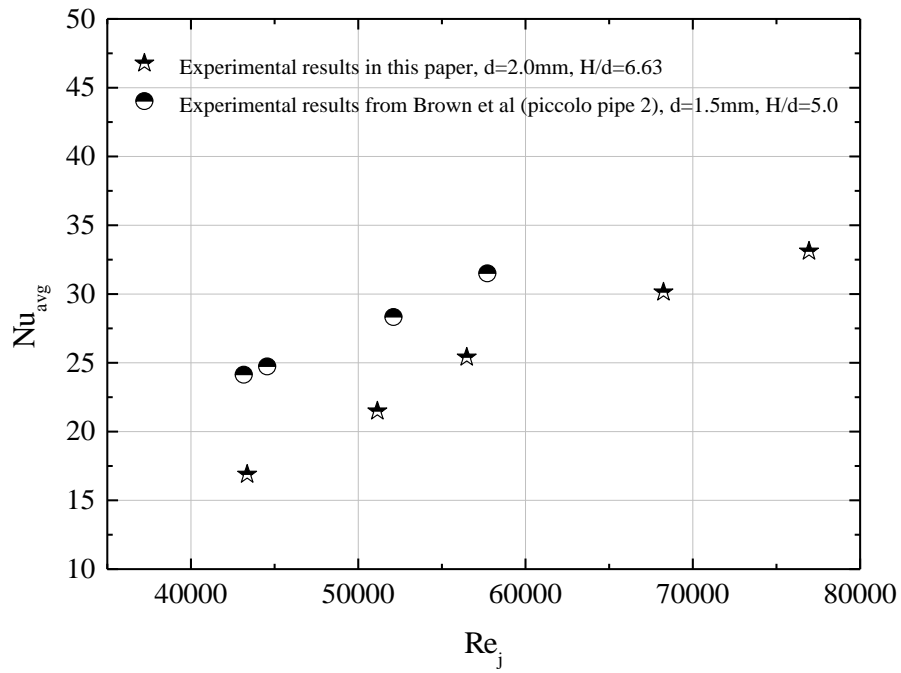
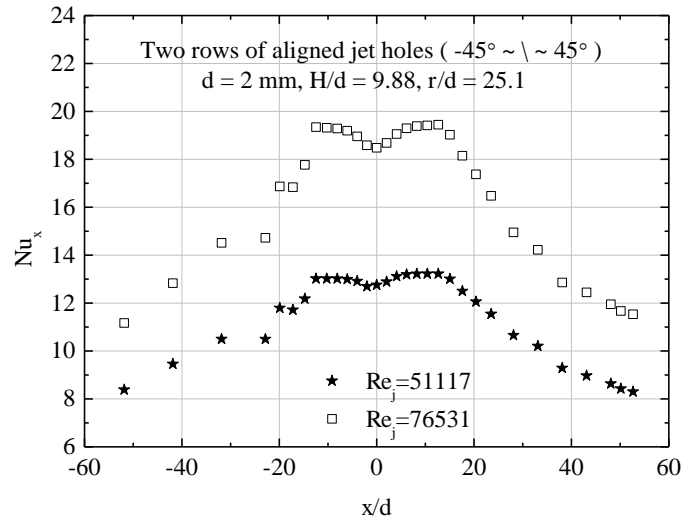
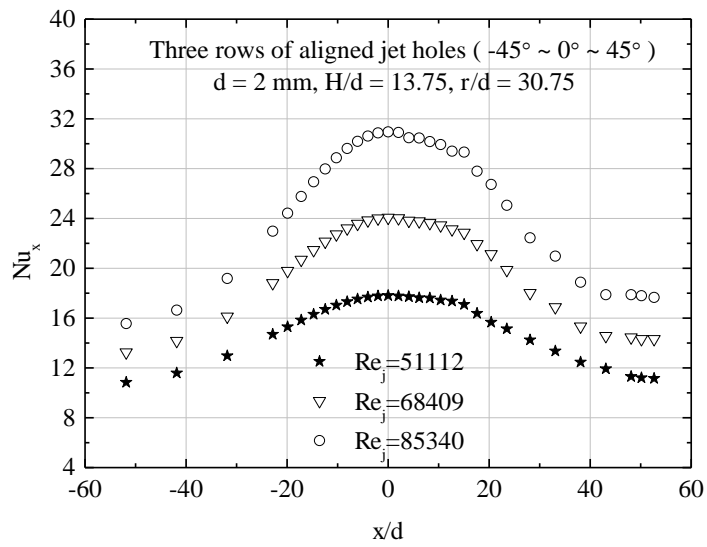


Fig. 8 Comparison and validation of the experimental results

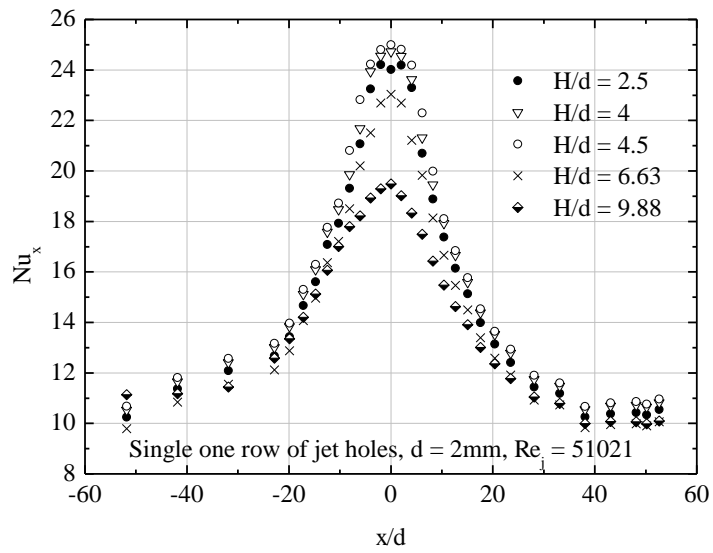


(a) two rows of aligned jet holes

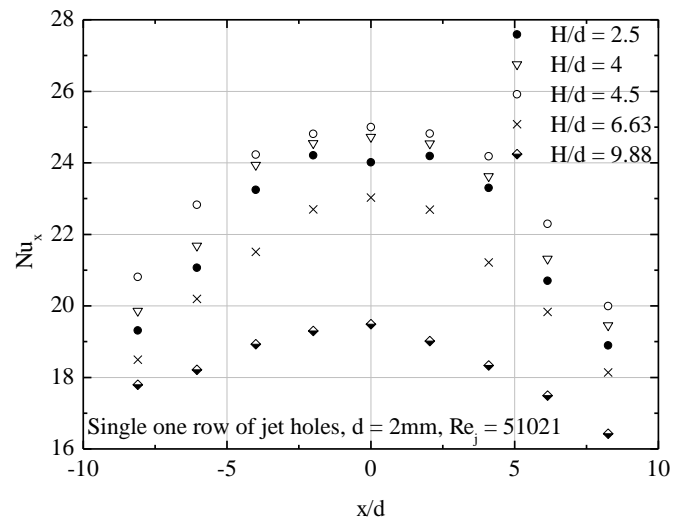


(b) three rows of aligned jet holes

Fig. 9 Influence of  $Re_j$  on  $Nu_x$  distribution in the chordwise direction



(a) the whole range



(b) local enlargement

Fig. 10 Influence of  $H/d$  on  $Nu_x$  distribution in the chordwise direction for single one row of jet holes

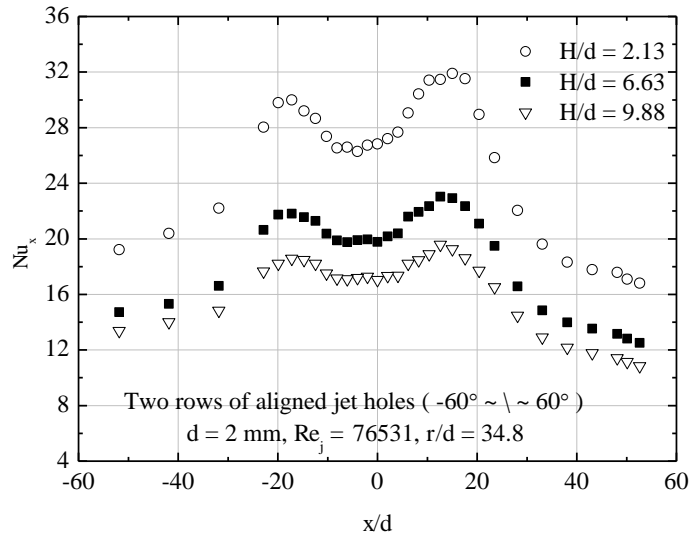


Fig. 11 Influence of  $H/d$  on  $Nu_x$  distribution in the chordwise direction for two rows of jet holes

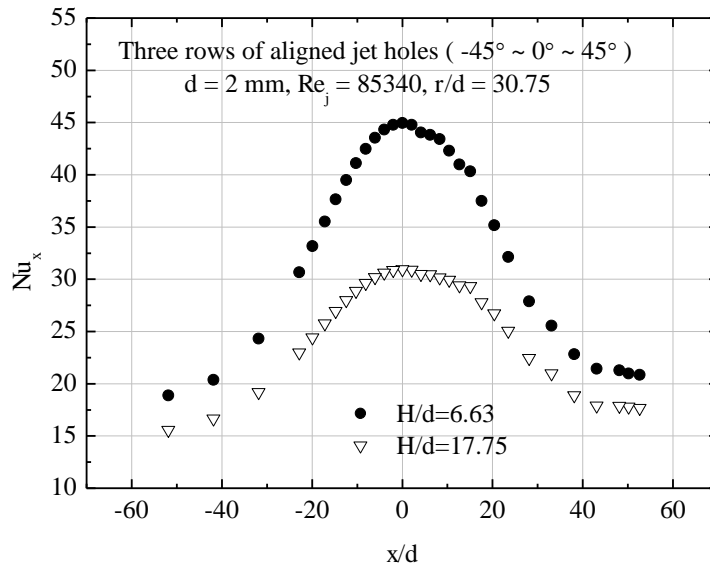


Fig. 12 Influence of  $H/d$  on  $Nu_x$  distribution in the chordwise direction for three rows of jet holes

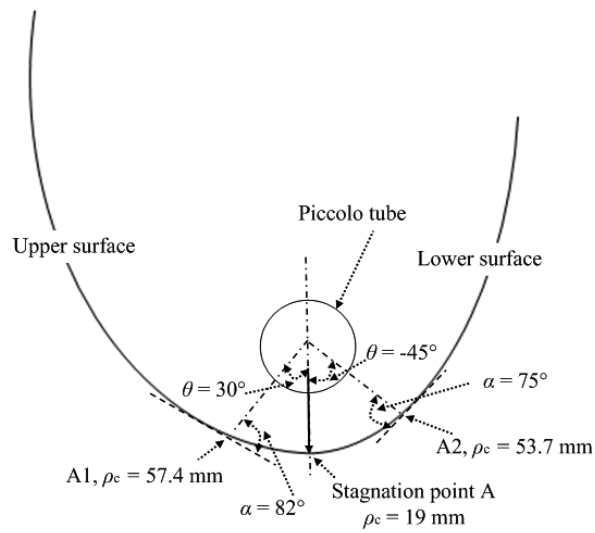
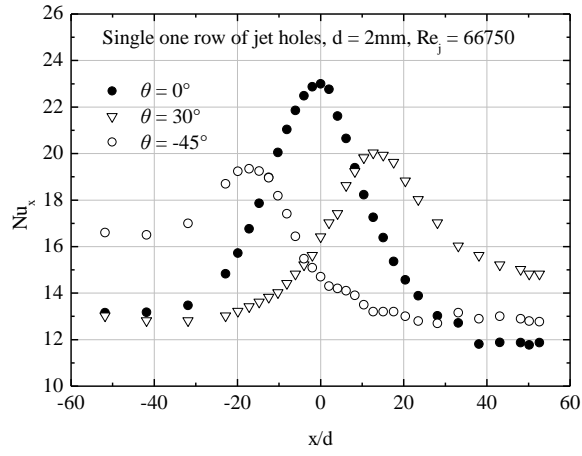
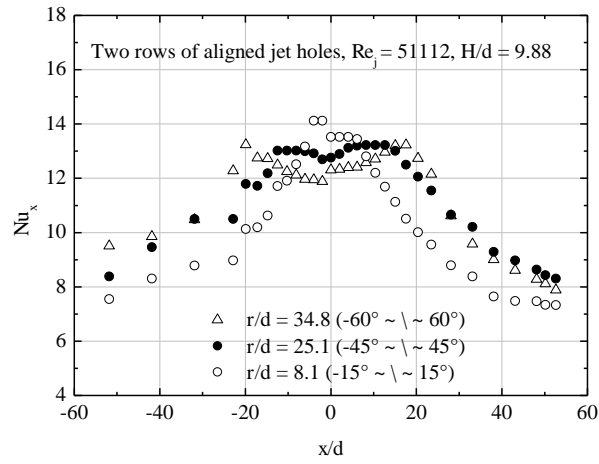


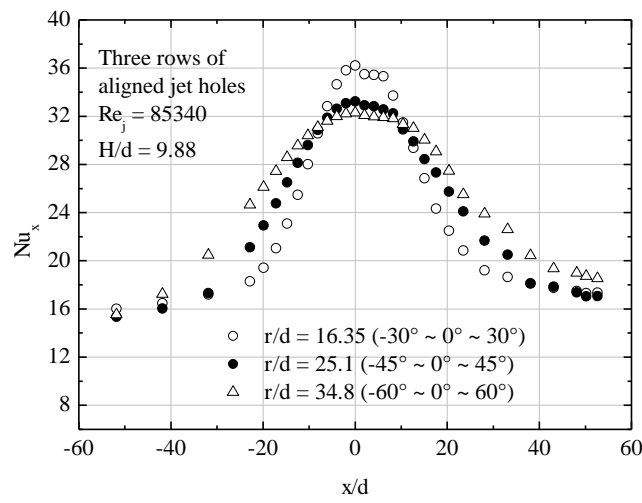
Fig. 13 Illustration of the circumferential angle of jet holes on the piccolo tube



(a) single one row of aligned jet holes



(b) two rows of aligned jet holes



(c) three rows of aligned jet holes

Fig. 14 Influence of circumferential angle of jet holes on  $Nu_x$  distribution in the chordwise direction